

# Electron-doping evolution of the low-energy spin excitations in the iron arsenide superconductor $\text{BaFe}_{2-x}\text{Ni}_x\text{As}_2$

Miaoyin Wang,<sup>1</sup> Huiqian Luo,<sup>2</sup> Jun Zhao,<sup>1</sup> Chenglin Zhang,<sup>1</sup> Meng Wang,<sup>2,1</sup> Karol Marty,<sup>3</sup> Songxue Chi,<sup>4</sup> Jeffrey W. Lynn,<sup>4</sup> Astrid Schneidewind,<sup>5,6</sup> Shiliang Li,<sup>2,\*</sup> and Pengcheng Dai<sup>1,2,3,†</sup>

<sup>1</sup>*Department of Physics and Astronomy, The University of Tennessee, Knoxville, Tennessee 37996-1200, USA*

<sup>2</sup>*Beijing National Laboratory for Condensed Matter Physics and Institute of Physics, Chinese Academy of Sciences, P.O. Box 603, Beijing 100190, China*

<sup>3</sup>*Neutron Scattering Science Division, Oak Ridge National Laboratory, Oak Ridge, Tennessee 37831-6393, USA*

<sup>4</sup>*NIST Center for Neutron Research, National Institute of Standards and Technology, Gaithersburg, Maryland 20899, USA*

<sup>5</sup>*Gemeinsame Forschergruppe HZB, Helmholtz-Zentrum Berlin für Materialien und Energie, D-14109 Berlin, Germany*

<sup>6</sup>*Forschungszentrum für Neutronenphysik und Neutronenoptik, TU München, D-85747 Garching, Germany*

(Received 14 February 2010; revised manuscript received 26 April 2010; published 24 May 2010)

We use elastic and inelastic neutron scattering to systematically investigate the evolution of the low-energy spin excitations of the iron arsenide superconductor  $\text{BaFe}_{2-x}\text{Ni}_x\text{As}_2$  as a function of nickel doping  $x$ . In the undoped state,  $\text{BaFe}_2\text{As}_2$  exhibits a tetragonal-to-orthorhombic structural phase transition and simultaneously develops a collinear antiferromagnetic (AF) order below  $T_N=143$  K. Upon electron doping of  $x=0.075$  to induce bulk superconductivity with  $T_c=12.2$  K, the AF ordering temperature reduces to  $T_N\approx 58$  K. We show that the appearance of bulk superconductivity in  $\text{BaFe}_{1.925}\text{Ni}_{0.075}\text{As}_2$  coincides with a dispersive neutron spin resonance in the spin excitation spectra and a reduction in the static ordered moment. For optimally doped  $\text{BaFe}_{1.9}\text{Ni}_{0.1}\text{As}_2$  ( $T_c=20$  K) and overdoped  $\text{BaFe}_{1.85}\text{Ni}_{0.15}\text{As}_2$  ( $T_c=14$  K) superconductors, the static AF long-range order is completely suppressed and the spin excitation spectra are dominated by a resonance and spin gap at lower energies. We determine the electron-doping dependence of the neutron spin resonance and spin gap energies and demonstrate that the three-dimensional nature of the resonance survives into the overdoped regime. If spin excitations are important for superconductivity, these results would suggest that the three-dimensional characters of the electronic superconducting gaps are prevalent throughout the phase diagram and may be critical for superconductivity in these materials.

DOI: [10.1103/PhysRevB.81.174524](https://doi.org/10.1103/PhysRevB.81.174524)

PACS number(s): 74.25.Ha, 74.70.-b, 78.70.Nx

## I. INTRODUCTION

An experimental determination of the doping evolution of the spin excitations in iron arsenide superconductors<sup>1-4</sup> is important for a comprehensive understanding of the role of magnetism in the superconductivity of these materials. Like high-transition temperature (high- $T_c$ ) copper oxides, the parent compounds of iron arsenide superconductors exhibit static antiferromagnetic (AF) long-range order with a collinear spin structure.<sup>5-8</sup> Although there is currently no consensus on a microscopic mechanism for superconductivity, spin excitations have been postulated by several theories to play a crucial role in the electron pairing and superconductivity of these materials.<sup>9-13</sup> In one class of unconventional microscopic theories for superconductivity, electron pairing in iron arsenide superconductors is mediated by quasiparticle excitations between sign-reversed holelike pockets around the  $\Gamma$  point and the electronlike Fermi pockets around the  $M$  point as shown in the inset of Fig. 1(a).<sup>14</sup> If this is indeed the case, spin excitations in the superconducting state should have a collective mode called the neutron spin resonance, whose energy is at (or slightly less than) the addition of the hole and electron superconducting gap energies [ $E=|\Delta(k+Q)+\Delta(k)|$ ], where  $Q$  is the AF ordering wave vector connecting the hole and electron Fermi pockets at the  $\Gamma$  and  $M$  points, respectively].<sup>15-18</sup> Although recent inelastic neutron scattering experiments have found the neutron spin resonance for different iron-based superconductors consistent with this

picture,<sup>19-27</sup> a surprising result has been found that the mode in the optimally doped  $\text{BaFe}_{1.9}\text{Ni}_{0.1}\text{As}_2$  ( $T_c=20$  K) has three-dimensional character as demonstrated by clear dispersion of the mode energy along the  $c$  axis.<sup>21,22</sup> These results are quite different from the two-dimensional nature of the resonance in copper oxide superconductors.<sup>28-33</sup> If spin excitations are important for superconductivity in iron arsenides, it would be interesting to systematically investigate the doping evolution of the resonance in  $\text{BaFe}_{2-x}\text{Ni}_x\text{As}_2$  and determine if the three-dimensional nature of the mode is a general phenomenon or specific only to the optimally doped materials. Furthermore, since spin waves in the AF-ordered parent compounds of  $(\text{Ba,Sr,Ca})\text{Fe}_2\text{As}_2$  have rather large anisotropy spin gaps at the AF zone center<sup>34-39</sup> and spin excitations in the optimally electron-doped superconducting samples are generally gapless in the nonsuperconducting normal state,<sup>20-22,26</sup> it would be important to see how spin waves in the parent compounds evolve as electrons are doped into the FeAs planes.

In this paper, we report our inelastic neutron scattering studies of the low-energy spin excitations in electron-doped  $\text{BaFe}_{2-x}\text{Ni}_x\text{As}_2$ , with  $x=0.075, 0.15$  [Fig. 1(a)], and compare and contrast them to the spin excitations observed at optimal doping and in the lightly doped regime. Before Ni doping,  $\text{BaFe}_2\text{As}_2$  exhibits simultaneous structural and magnetic phase transitions below  $T_s=T_N=143$  K, changing the crystal lattice symmetry from the high-temperature tetragonal to the low-temperature orthorhombic phase.<sup>7</sup> Upon doping elec-

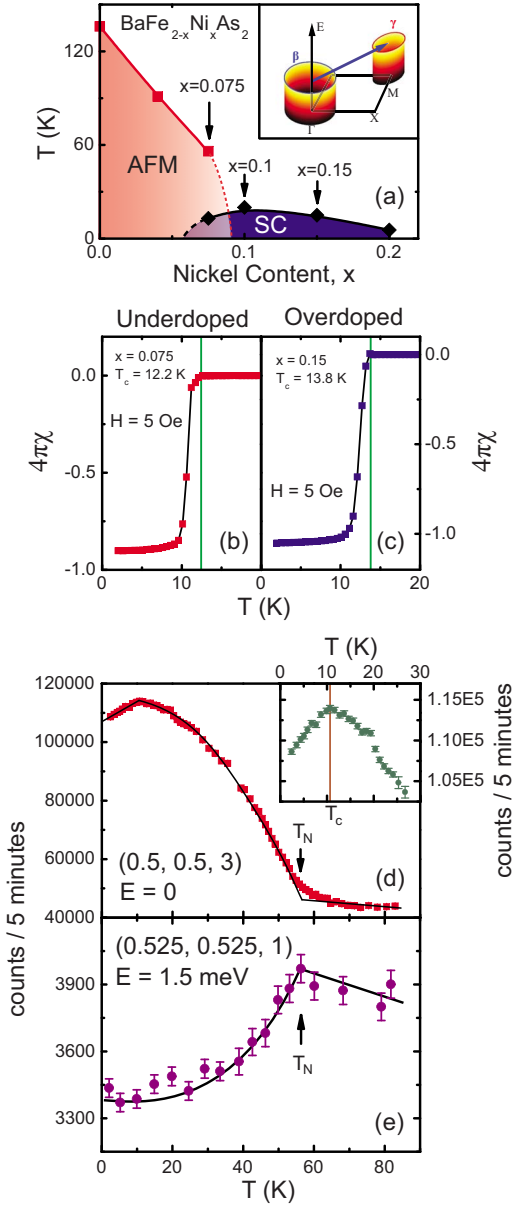


FIG. 1. (Color online) (a) Electronic phase diagram of  $\text{BaFe}_{2-x}\text{Ni}_x\text{As}_2$  as determined from our previous (Refs. 21, 22, and 43) and current neutron scattering works. Inset shows schematic illustration of quasiparticle excitations from the hole pocket at the  $\Gamma$  point to the electron pocket at the  $M$  point as predicted by various theories (Refs. 15–18). [(b) and (c)] Temperature dependence of the Meissner and shielding signals on thin slabs of  $\text{BaFe}_{1.925}\text{Ni}_{0.075}\text{As}_2$  ( $V = 2.17 \times 0.76 \times 0.058$  mm<sup>3</sup> and mass 0.62 mg) and  $\text{BaFe}_{1.85}\text{Ni}_{0.15}\text{As}_2$  ( $V = 4.16 \times 1.16 \times 0.092$  mm<sup>3</sup> and mass 2.88 mg). These measurements were taken in zero-field cooling (ZFC) with 5 Oe applied field along the thin slab's direction. The superconducting volume fractions were estimated to be about 100% for both samples. (d) Temperature dependence of the  $Q = (0.5, 0.5, 3)$  magnetic Bragg peak in  $\text{BaFe}_{1.925}\text{Ni}_{0.075}\text{As}_2$ , showing a clear anomaly at  $T_N$  and  $T_c$ . Inset shows an expanded view of the  $Q = (0.5, 0.5, 3)$  magnetic Bragg peak near  $T_c$ . (e) Temperature dependence of the quasielastic scattering at  $E = 1.5$  meV and  $Q = (0.525, 0.525, 1)$  shows a clear anomaly at  $T_N = 58$  K. The rather high background scattering in (e) may be due to the fact that the probed energy is too close to the elastic scattering.

trons via either Co or Ni substitution for Fe, the structural and magnetic phase transitions are separated.<sup>40–42</sup> For  $x = 0.04$  Ni doping, the structural and magnetic phase transition temperatures of  $\text{BaFe}_{1.96}\text{Ni}_{0.04}\text{As}_2$  become near 97 and 91 K, respectively.<sup>43</sup> In addition, three-dimensional spin waves in  $\text{BaFe}_2\text{As}_2$  change into quasi-two-dimensional spin excitations for  $\text{BaFe}_{1.96}\text{Ni}_{0.04}\text{As}_2$  with no evidence for the neutron spin resonance<sup>43</sup> or bulk superconductivity.<sup>4</sup> By increasing the Ni doping  $x$  to 0.075 to form  $\text{BaFe}_{1.925}\text{Ni}_{0.075}\text{As}_2$  [Fig. 1(a)], bulk superconductivity appears at  $T_c = 12.2$  K [Fig. 1(b)] and the Néel temperature of the material is now reduced to  $T_N \approx 58$  K [Figs. 1(d) and 1(e)]. Our inelastic neutron scattering experiments show the presence of a three-dimensional neutron spin resonance with distinct energies at the AF wave vectors  $Q = (0.5, 0.5, 0)$  and  $(0.5, 0.5, 1)$ , quite similar to that of the optimally doped  $\text{BaFe}_{1.9}\text{Ni}_{0.1}\text{As}_2$ .<sup>21,22</sup> The intensity gain of the mode below  $T_c$  is compensated by opening a pseudo- (not complete) spin gap at lower energies and reduction in the static AF order [see inset in Fig. 1(d)].

To study the doping evolution of the resonance, we also carried out inelastic neutron scattering experiments on overdoped  $\text{BaFe}_{1.85}\text{Ni}_{0.15}\text{As}_2$  [ $T_c = 14$  K, Fig. 1(c)] and found that the energy of the mode is approximately proportional to  $T_c$ . Our elastic neutron scattering measurements indicate that the static antiferromagnetism has been completely suppressed, while the neutron spin resonance in the superconducting state exhibits similar dispersion along the  $c$  axis as the underdoped and optimally doped materials. This suggests that the three-dimensional nature of the resonance energy and its associated superconducting gap energy  $\Delta$  are prevalent throughout the superconducting electronic phase diagram. These results can also provide information needed for calculating the electron-doping dependence of the AF coupling between the layers and estimating the doping dependence of the superconducting gap energy.

## II. EXPERIMENTAL DETAILS

In two recent inelastic neutron scattering experiments on underdoped  $\text{BaFe}_{1.906}\text{Co}_{0.094}\text{As}_2$  ( $T_c = 15$  K) (Ref. 24) and  $\text{BaFe}_{1.92}\text{Co}_{0.08}\text{As}_2$  ( $T_c = 11$  K),<sup>25</sup> static AF order was found to coexist with superconductivity and cooling below  $T_c$ 's in these samples induced a weak neutron spin resonance in the magnetic excitation spectra at the expense of elastic magnetic scattering.<sup>24,25</sup> For  $\text{BaFe}_{2-x}\text{Ni}_x\text{As}_2$ , bulk superconductivity appears only when  $x \geq 0.05$ .<sup>4</sup> To compare the electronic phase diagram of  $\text{BaFe}_{2-x}\text{Ni}_x\text{As}_2$  to Co-doped materials and see the effect of superconductivity on the spin excitations, we chose to study underdoped  $\text{BaFe}_{1.925}\text{Ni}_{0.075}\text{As}_2$  (where Ni concentration is nominal, which is close to the actual Ni-value based on previous work<sup>3,4</sup>) and overdoped  $\text{BaFe}_{1.85}\text{Ni}_{0.15}\text{As}_2$  superconductors. The temperature dependence of the susceptibility in Figs. 1(b) and 1(c) show  $T_c$ 's of 12.2 and 14 K for  $\text{BaFe}_{1.925}\text{Ni}_{0.075}\text{As}_2$  and  $\text{BaFe}_{1.85}\text{Ni}_{0.15}\text{As}_2$ , respectively. Based on these data, we estimate that the superconducting volume fractions for both samples are approximately 100%. This is consistent with the overall electronic phase diagram from the heat capacity measurements.<sup>4</sup>

We grew single crystals of  $\text{BaFe}_{2-x}\text{Ni}_x\text{As}_2$ , with  $x = 0.075, 0.15$ , using the self-flux method.<sup>3</sup> Our neutron scat-

tering experiments were carried out on the HB-3, HB-1 thermal triple-axis spectrometers at the high-flux-isotope reactor (HFIR), Oak Ridge National Laboratory,<sup>34</sup> the BT-7 thermal triple-axis spectrometer at the NIST Center for Neutron Research,<sup>22</sup> and the PANDA cold triple-axis spectrometer at the Forschungsneutronenquelle Heinz Maier-Leibnitz (FRM-II), TU München.<sup>21</sup> We defined the wave vector  $Q$  at  $(q_x, q_y, q_z)$  as  $(H, K, L) = (q_x a / 2\pi, q_y b / 2\pi, q_z c / 2\pi)$  reciprocal lattice units (rlu) using the tetragonal nuclear unit cell, where  $a = 3.89$  Å,  $b = 3.89$  Å, and  $c = 12.77$  Å. We coaligned about 6 g for each of the  $x = 0.075, 0.15$  samples of  $\text{BaFe}_{2-x}\text{Ni}_x\text{As}_2$  in the  $[H, H, L]$  horizontal scattering plane (with mosaicity  $\sim 3^\circ$  for each of the crystal assembly) and put our samples inside either a closed cycle refrigerator or a liquid He cryostat.

For thermal triple-axis measurements on HB-1, HB-3, and BT-7, we used pyrolytic graphite (PG) as monochromator and analyzer with typical collimations of open- $40' - S - 40' - 120'$ . The final neutron energy was chosen to be either  $E_f = 13.5$  meV or  $E_f = 14.7$  meV with a PG filter before the analyzer. For cold triple-axis measurements on PANDA, we chose a final neutron energy of  $E_f = 5.0$  meV with a cooled Be filter in front of the analyzer. We used both horizontal and vertical focusing PG monochromator and analyzer with no collimators. We also used a  $E_f = 13.5$  meV setup with a PG filter in one of the PANDA measurements. For  $E_f = 5.0$  meV and  $E_f = 13.5$  meV setups, the instrumental energy resolutions are about 0.15 and 1.2 meV, respectively.

### III. RESULTS AND DISCUSSIONS

We first describe our elastic and quasielastic neutron scattering results on the underdoped  $\text{BaFe}_{1.925}\text{Ni}_{0.075}\text{As}_2$ . Consistent with earlier results on underdoped  $\text{BaFe}_{1.906}\text{Co}_{0.094}\text{As}_2$  (Ref. 24) and  $\text{BaFe}_{1.92}\text{Co}_{0.08}\text{As}_2$  (Ref. 25), the AF structure of the  $\text{BaFe}_{1.925}\text{Ni}_{0.075}\text{As}_2$  sample reported here is identical to the undoped parent compound but with a Néel  $T_N \approx 58$  K [Fig. 1(c)]. The temperature dependence of the quasielastic scattering at  $Q = (0.525, 0.525, 1)$  and  $E = 1.5$  meV shows a clear kink below  $\sim 58$  K, thus confirming the Néel temperature of the system. The inset in Fig. 1(d) shows the expanded temperature dependence of the AF Bragg peak intensity at  $Q = (0.5, 0.5, 3)$ . The scattering decreases with decreasing temperature at the onset of  $T_c$ , suggesting that the static moment competes with superconductivity similar to the Co-doped materials.<sup>24,25</sup>

To see if there is a neutron spin resonance mode in underdoped  $\text{BaFe}_{1.925}\text{Ni}_{0.075}\text{As}_2$  and to compare its  $c$ -axis dispersion with optimally doped  $\text{BaFe}_{1.9}\text{Ni}_{0.1}\text{As}_2$ ,<sup>21</sup> we carried out constant- $Q$  scans at  $Q = (0.5, 0.5, 0)$  and  $(0.5, 0.5, 1)$  above and below the superconducting transition temperature  $T_c$ . Figure 2(a) shows the raw data collected on the HB-3 triple-axis spectrometer at the signal  $Q = (0.5, 0.5, 0)$  and background  $Q = (0.7, 0.7, 0)$  positions. There is clear intensity gain at  $Q = (0.5, 0.5, 0)$  near  $E = 7$  meV below  $T_c$  at the expense of spectral weight loss below  $\sim 4$  meV. The temperature difference spectrum between 2 and 20 K in Fig. 2(b) confirms the presence of the mode at  $E = 7$  meV below  $T_c$  and a reduction in spectral weight below 4 meV. The open

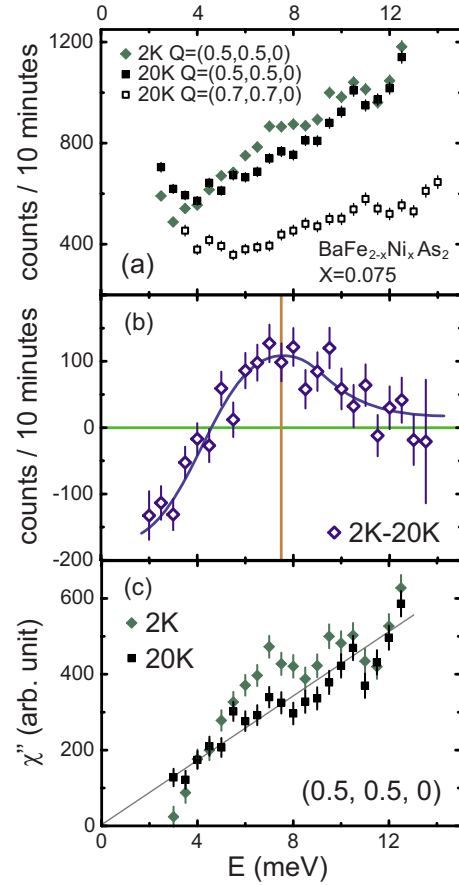


FIG. 2. (Color online) (a) Energy scans at  $Q = (0.5, 0.5, 0)$  (signal) and  $Q = (0.7, 0.7, 0)$  (background) positions above and below  $T_c$  for  $\text{BaFe}_{1.925}\text{Ni}_{0.075}\text{As}_2$ . (b) Temperature difference plot (low temperature minus high temperature) in  $S(Q, \omega)$  shows a clear neutron spin resonance at  $E = 7$  meV below  $T_c$ . Solid line is a guide to the eye. (c) Estimation of the temperature dependence of  $\chi''(Q, \omega)$  above and below  $T_c$  using the background determined both from constant-energy scans and from constant- $Q$  scans at background position.

squares in Fig. 2(a) show the energy dependence of the background scattering at  $Q = (0.7, 0.7, 0)$ .

Figure 3 summarizes constant-energy scans at  $E = 7$  and 3 meV along the  $[H, H, 0]$  direction. At the resonance energy, the scattering shows a well-defined peak centered at  $Q = (0.5, 0.5, 0)$  that increases in intensity below  $T_c$  [Fig. 3(a)]. Figure 3(b) shows the temperature difference plot which confirms that the intensity gain below  $T_c$  in Fig. 2(a) occurs at  $Q = (0.5, 0.5, 0)$ . Similarly, constant-energy scans at  $E = 3$  meV above and below  $T_c$  in Fig. 3(c) reveal clear normal state magnetic scattering that is not completely suppressed (gapped) below  $T_c$  at  $E = 3$  meV. Since the energy resolution of these thermal triple-axis measurements is about 1.5 meV full width at half maximum, we simply do not know if the system is gapped at energies below 2.5 meV in the superconducting state. Future cold neutron triple-axis measurements are necessary to resolve this issue.

Figure 2(c) shows our estimation of the energy dependence of the dynamic susceptibility  $\chi''(Q, \omega)$  above and below  $T_c$ , obtained by subtracting the background and correct-

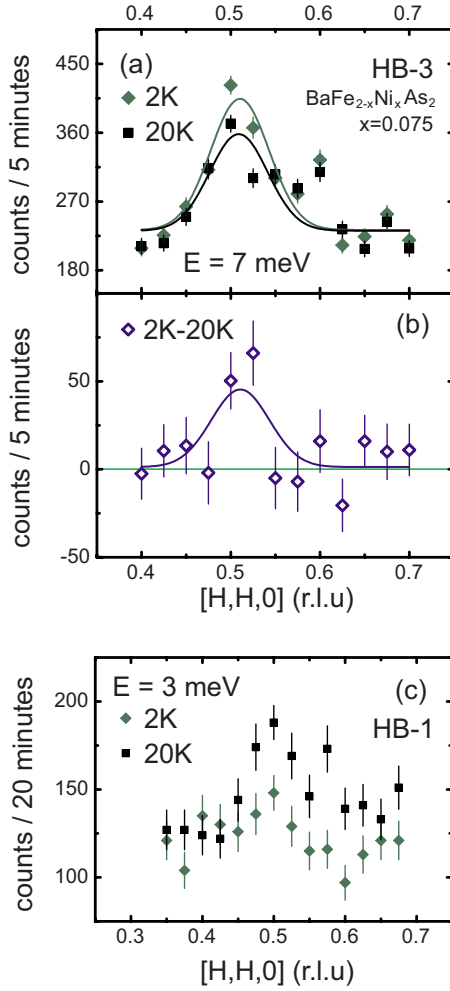


FIG. 3. (Color online) (a) Constant-energy scans near the resonance energy ( $E=7$  meV) along the  $(H,H,0)$  direction across  $T_c$  for  $\text{BaFe}_{1.925}\text{Ni}_{0.075}\text{As}_2$ . The scattering clearly increases at the  $Q=(0.5,0.5,0)$  below  $T_c$ . The small peak at  $Q=(0.6,0.6,0)$  is spurious. (b) Temperature difference plot confirms the intensity gain at  $Q=(0.5,0.5,0)$  below  $T_c$ . (c) Wave-vector scans at  $E=3$  meV. Here, the scattering at  $Q=(0.5,0.5,0)$  decreases below  $T_c$  but there is no spin gap at  $E=3$  meV. The scattering near  $Q=(0.57,0.57,0)$  in the normal state is spurious.

ing for the Bose population factor using  $\chi''(Q, \omega)=[1-\exp(-\hbar\omega/k_B T)]S(Q, \omega)$ , where  $E=\hbar\omega$ . While the normal state susceptibility appears to increase linearly with energy, superconductivity rearranges the spectrum, creating a (pseudo) spin gap below 4 meV (defined as a suppression of spin fluctuations) and a neutron spin resonance at  $E=7$  meV for in-phase spin fluctuations along the  $c$  axis ( $L=0$ ).

To investigate the behavior for the out-of-phase spin fluctuations along the  $c$  axis, we plot in Fig. 4(a) constant- $Q$  scans at  $Q=(0.5,0.5,1)$  above and below  $T_c$ . Figure 4(b) shows the temperature difference plot, and a comparison of Figs. 4(b) and 2(b) immediately reveals that the neutron spin resonance has moved from  $E=7$  meV at  $Q=(0.5,0.5,0)$  to  $E=5$  meV at  $Q=(0.5,0.5,1)$ . Note in particular that for  $Q=(0.5,0.5,0)$ , there is essentially no change with temperature for the scattering at 5 meV (Fig. 2), which is where the maximum in intensity occurs at the  $Q=(0.5,0.5,1)$  position.

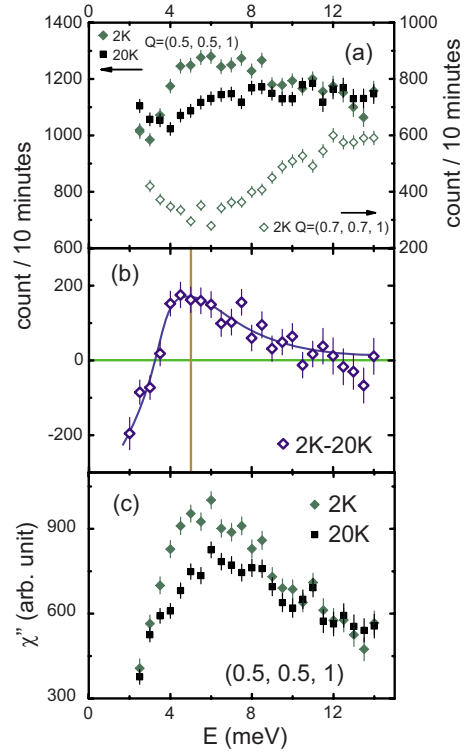


FIG. 4. (Color online) (a) Constant- $Q$  scans at  $Q=(0.5,0.5,1)$  above and below  $T_c$  for  $\text{BaFe}_{1.925}\text{Ni}_{0.075}\text{As}_2$ . The scattering shows clear asymmetric enhancement around  $E=5$  meV below  $T_c$ . (b) Temperature difference plot reveals a neutron spin resonance at  $E=5$  meV, clearly below the energy of the mode at  $Q=(0.5,0.5,0)$  as shown in Fig. 2.

This is compelling evidence that the neutron spin resonance is dispersive for both underdoped and optimally doped  $\text{BaFe}_{2-x}\text{Ni}_x\text{As}_2$ . Figure 4(c) plots our estimated energy dependence of  $\chi''(Q, \omega)$  above and below  $T_c$ .

Figure 5 shows constant-energy scans along the  $[H,H,1]$  direction and the temperature difference data between 2 and 20 K for  $E=2.5, 5.5$  meV. Similar to the  $[H,H,0]$  scans in Fig. 3, we find that superconductivity only reduces but does not completely suppress the magnetic scattering at  $E=2.5$  meV [Figs. 5(a) and 5(b)]. Similarly, the scattering near the resonance energy at  $E=5.5$  meV shows a clear increase below  $T_c$ . To test if the intensity gain at  $E=7$  and  $Q=(0.5,0.5,0)$  is responding to superconductivity, we show in Fig. 6 the temperature dependence of the scattering, which clearly increases below  $T_c$  consistent with the temperature dependence of the neutron spin resonance.<sup>19–22,24–26</sup>

To determine the  $c$ -axis modulation of the spin excitations at different temperatures and energies, we show in Figs. 7–9 constant-energy scans along the  $Q=(0.5,0.5,L)$  (signal) and  $Q=(0.7,0.7,L)$  (background) directions at  $E=3, 5.5,$  and  $7$  meV, respectively. Inspection of the data immediately suggests that the scattering is antiferromagnetically correlated between the layers along the  $c$  axis. To model the AF spin correlations along the  $c$  axis, we assume their structure factor is similar to that of<sup>44</sup>  $f(Q_c)=F^2(Q)[S_0+\sum\{S_{L_0}\exp[-(L-L_0)^2/2\sigma^2]\}]$ , where  $F(Q)$  is the magnetic form factor,<sup>45</sup>  $L=Q_c c/2\pi$ ,  $L_0=\pm 1, \pm 3, \dots$ ,  $\sigma$  is the width of the Gaussian

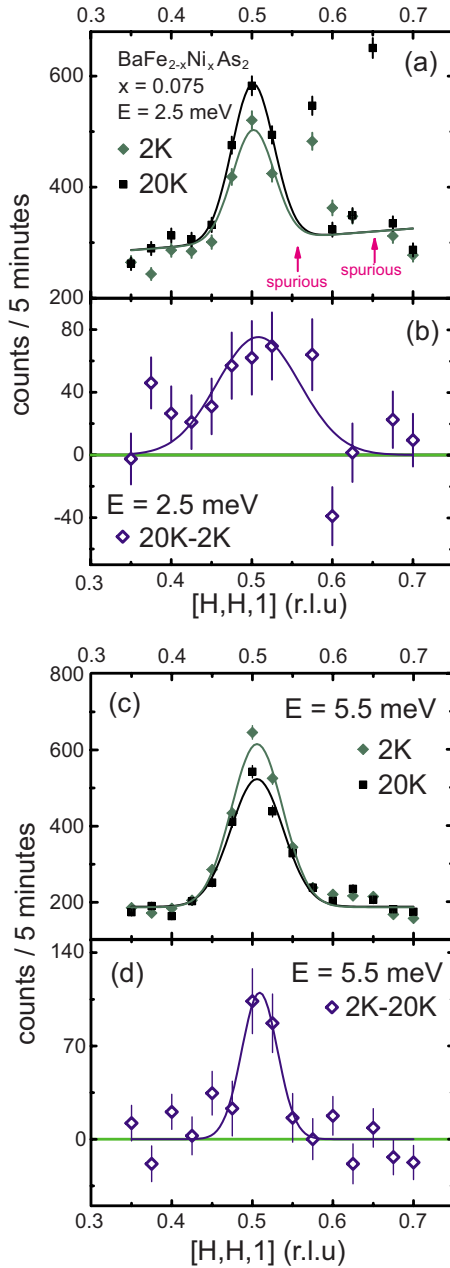


FIG. 5. (Color online) (a)  $Q$ -scans along the  $(H, H, 1)$  direction at  $E = 2.5$  meV above and below  $T_c$  for  $\text{BaFe}_{1.925}\text{Ni}_{0.075}\text{As}_2$ . (b) Temperature difference plot shows that the scattering at  $Q = (0.5, 0.5, 1)$  and  $E = 2.5$  meV decreases below  $T_c$ . (c) Identical  $Q$ -scans across  $T_c$  at the resonance energy of  $E = 5.5$  meV. The scattering enhances below  $T_c$ . (d) Temperature difference plot between 2 and 20 K, showing clear field-induced scattering below  $T_c$  at  $Q = (0.5, 0.5, 1)$ .

which gives the correlation length of the spin excitations along the  $c$  axis, and  $S_0$  and  $S_{L_0}$  are fitting parameters for constant magnetic rod scattering along any  $L$  and maximum magnetic intensity at odd values of  $L$ , respectively.

Figure 7 shows the temperature dependence of the magnetic scattering at  $E = 3$  meV along the  $c$  axis. Starting from 2 and 20 K in Fig. 7(a), we see two clear peaks centered around  $Q = (0.5, 0.5, 1)$  and  $(0.5, 0.5, -1)$  above the background. Fourier transforms of the fitted Gaussian peaks give

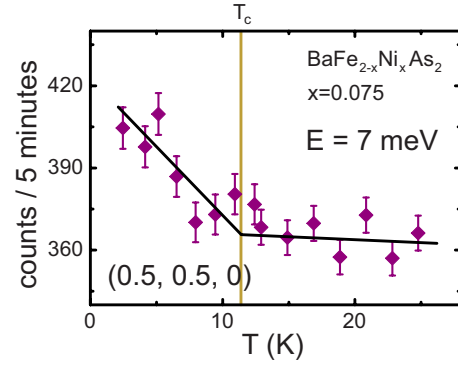


FIG. 6. (Color online) (a) Temperature dependence of the  $E = 7$  meV scattering at  $Q = (0.5, 0.5, 0)$  for  $\text{BaFe}_{1.925}\text{Ni}_{0.075}\text{As}_2$ . The scattering increases in intensity below  $T_c$  of 12.2 K.

a  $c$ -axis spin correlation length of  $\sim 14$  Å [Fig. 7(b)]. Upon increasing temperature to 50 and 70 K, the magnetic peaks at  $Q = (0.5, 0.5, 1)$  and  $(0.5, 0.5, -1)$  reduce in intensity but the  $c$ -axis spin-spin correlations appear not to be affected [Fig. 7(c)]. To test if the magnetic scattering below  $T_N$  simply follows the Bose population factor as expected for classical spin waves excitations, we show in Fig. 7(d) the temperature dependence of the magnetic scattering normalized to the scattering at 2 K. The observed magnetic scattering clearly does not obey the Bose population factor, suggesting that the spin excitations in the doped materials are not simple spin waves, in contrast to the (undoped) parent compounds.<sup>34</sup>

To probe the  $L$  dependence of the magnetic scattering at the neutron spin resonance energies, we show in Figs. 8 and 9 constant-energy scans at  $E = 5.5$  and 7 meV, respectively. Consistent with constant-energy scan data at  $E = 3$  meV (Fig. 7), the magnetic scattering is still centered at  $L = \pm 1, \pm 3$  positions and superconductivity has a relatively small effect on the overall magnetic scattering. Comparison of Figs. 2, 4, 8, and 9 reveals that the neutron spin resonance so clearly illustrated in the temperature difference scattering is a rather subtle effect that occurs at both  $L = 0$  and  $L = 1$  [Figs. 8(c) and 9(a)]. On warming to 50 and 70 K, the magnetic scattering decreases but the  $c$ -axis spin correlation length of  $\sim 14$  Å appears to be fairly temperature independent. The solid line in Fig. 8(a) shows Gaussian fits to the data at 70 K, which appear to describe the data reasonably well. However, the decrease in the magnetic scattering along the  $c$ -axis direction clearly falls off faster than just the  $\text{Fe}^{2+}$  form factor at temperatures near  $T_c$  as shown in Fig. 8(c).<sup>45</sup> Similar results are also seen for spin excitations at  $E = 7$  meV as shown in Fig. 9(a) near  $T_c$ . If we assume that the spins prefer to lie in the  $a$ - $b$  plane as is the case for the AF undoped system, an additional reduction in intensity is expected due to the neutron spin-Fe-spin orientation factor. This suggests that the spins prefer to lie within the tetragonal  $a$ - $b$  plane even in superconducting samples at low temperatures.

Having described our comprehensive measurements on the underdoped  $\text{BaFe}_{1.925}\text{Ni}_{0.075}\text{As}_2$ , we now discuss inelastic neutron scattering experiments on the overdoped  $\text{BaFe}_{1.85}\text{Ni}_{0.15}\text{As}_2$  [Figs. 1(a) and 1(c)], where the static AF order is completely suppressed. These measurements were carried out on the PANDA cold triple-axis spectrometer. Fig-

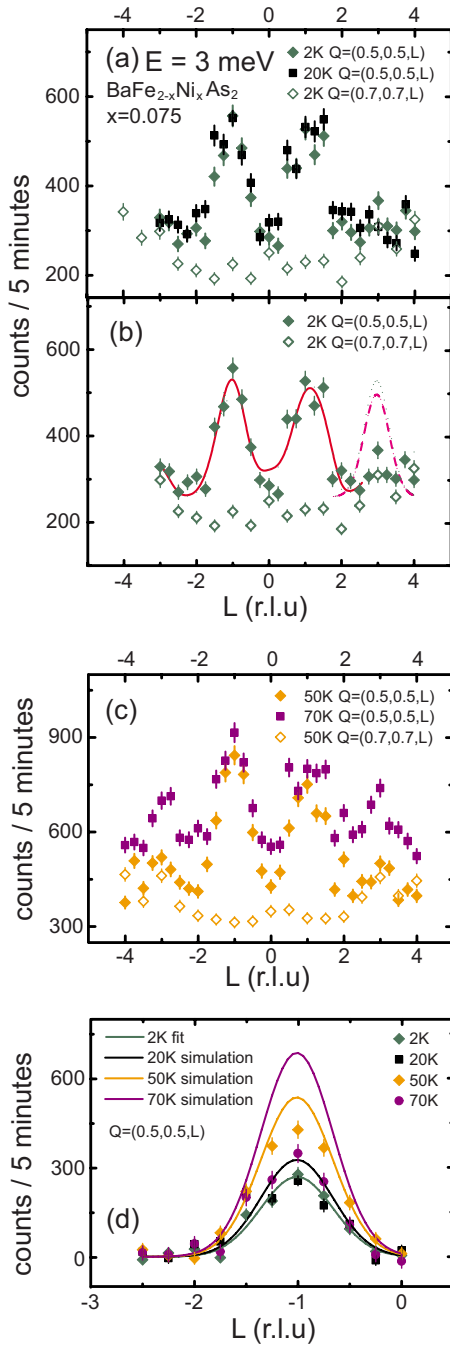


FIG. 7. (Color online) Constant-energy scans along the  $(0.5, 0.5, L)$  (signal) and  $(0.7, 0.7, L)$  (background) directions at  $E = 3$  meV and various temperatures. (a) The scattering at 2 and 20 K shows well-defined peaks centered at  $L = \pm 1$ . Fourier transform of these peaks gives a  $c$ -axis spin-spin correlation length of  $\sim 14$  Å. (b) Signal and background scattering at 2 K. Solid lines are Gaussian fits to the data. Dashed line shows the expected magnetic scattering at  $Q = (0.5, 0.5, 3)$  assuming  $\text{Fe}^{2+}$  form factor. The absence of clear peaks at  $L = \pm 3$  suggests that magnetic scattering in  $\text{BaFe}_{1.925}\text{Ni}_{0.075}\text{As}_2$  damps out much faster than expected. (c) Similar scans at 50 and 70 K. (d) Solid lines show the effect of Bose population factor as a function of increasing temperature if one normalizes the magnetic scattering above background at 2 K. The magnetic intensity changes in the system clearly do not obey the Bose statistics, indicating that the scattering is not spin waves.

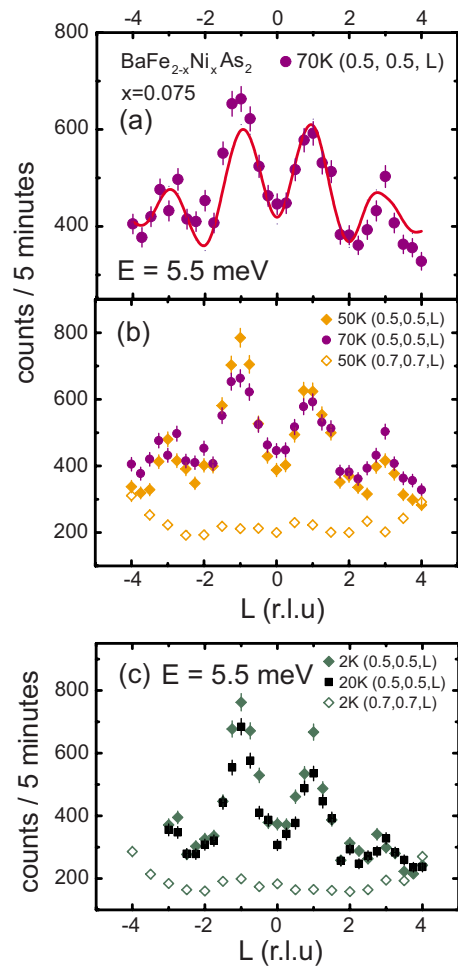


FIG. 8. (Color online) Constant-energy scans along the  $(0.5, 0.5, L)$  (signal) and  $(0.7, 0.7, L)$  (background) directions at the resonance energy of  $E = 5.5$  meV and various temperatures. (a)  $c$ -axis scattering at 70 K. Solid line shows the Gaussian fits to the data using  $\text{Fe}^{2+}$  form factor, which describes the data reasonably well. (b) Signal and background scattering at 50 K. The data again show clear peaks at  $L = \pm 1$  but much weaker peaks at  $L = \pm 3$ . (c) Signal and background scattering at 2 and 20 K. Superconductivity clearly enhances magnetic scattering at  $L = 0$  and  $L = \pm 1$ . The spin-spin correlation length is again about 14 Å and is weakly temperature dependent in the probed temperature range (2–70 K).

ure 10 summarizes the constant- $Q$  scans at  $Q = (0.5, 0.5, 0)$  and  $(0.5, 0.5, 1)$  below and above  $T_c$ . Using  $E_f = 5$  meV, we find in Figs. 10(b) and 10(d) that the neutron spin resonance occurs at  $E = 6$  meV for  $Q = (0.5, 0.5, 1)$ . Since the effect of the Bose factor for temperatures between 4 and 20 K is not so important for spin excitations with energies near 6 meV, the intensity gain at  $Q = (0.5, 0.5, 1)$  below  $T_c$  in Fig. 10(d) must arise from the increased  $\chi''(Q, \omega)$ . Similar scans at  $Q = (0.5, 0.5, 0)$  reveal clear scattering intensity enhancement above  $E = 5$  meV [Figs. 10(a) and 10(c)]. However, kinematic constraints with the  $E_f = 5$  meV spectrometer configuration did not allow a conclusive determination of the resonance energy. Figure 10(g) shows identical scans carried out with  $E_f = 13.5$  meV. Inspection of Figs. 10(g) and 10(h) indicates that the resonance energy at  $Q = (0.5, 0.5, 0)$  is now shifted to  $E = 8$  meV. To estimate the spin gap values in the

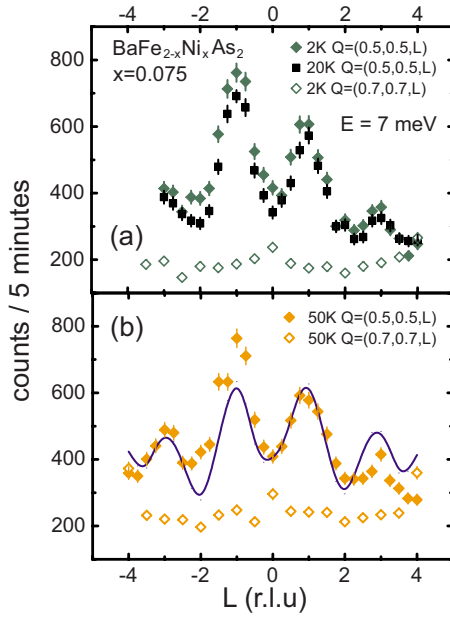


FIG. 9. (Color online)  $L$  dependence of the magnetic scattering for  $\text{BaFe}_{1.925}\text{Ni}_{0.075}\text{As}_2$ . (a) Identical scans as Fig. 8 except we now change the excitation energy to  $E=7$  meV. Comparison of the 2 and 20 K data here indicates that the magnetic scattering enhancement below  $T_c$  at  $L=0$  is larger than that at  $L=1$ . (b) Signal and background scattering at 50 K. Solid line shows the expected  $L$  dependence of the magnetic scattering assuming simple  $\text{Fe}^{2+}$  form factor, which clearly fails to describe the data.

superconducting state of  $\text{BaFe}_{1.85}\text{Ni}_{0.15}\text{As}_2$  at  $Q=(0.5,0.5,0)$  and  $(0.5,0.5,1)$ , we plot in Figs. 10(e) and 10(f)  $\chi''(Q,\omega)$  at temperatures above and below  $T_c$ , obtained by subtracting the backgrounds and correcting for the Bose population factor in Figs. 10(a) and 10(b). It is clear that spin excitation spectra have spin gaps in the superconducting state similar to previous work on optimally doped  $\text{BaFe}_{1.85}\text{Ni}_{0.15}\text{As}_2$ .<sup>22</sup>

To confirm the presence of a spin gap in the superconducting state of  $\text{BaFe}_{1.85}\text{Ni}_{0.15}\text{As}_2$ , we took constant-energy scans along the  $[H,H,0]$  and  $[H,H,1]$  directions above and below  $T_c$  for  $E=1$  meV. Figures 11(a) and 11(b) show that spin excitations of  $\text{BaFe}_{1.85}\text{Ni}_{0.15}\text{As}_2$  are gapless in the normal state for both  $L=0$  and 1 rlu. On cooling to the superconducting state at 4 K, the broad peaks centered at  $Q=(0.5,0.5,0)$  and  $(0.5,0.5,1)$  are suppressed and the scattering become featureless. This is consistent with constant- $Q$  scans in Fig. 10, where  $\chi''(Q,\omega)$  opens a spin gap below  $\sim 2.5$  meV. Assuming that the background does not change substantially between 20 and 4 K [Figs. 11(a) and 11(b)] and the low-temperature scattering at  $E=1$  meV is entirely non-magnetic, the difference plots between 20 and 4 K shown in Figs. 11(c) and 11(d) demonstrate that the normal state magnetic scattering is broad and centered at  $Q=(0.5,0.5,0)$  and  $(0.5,0.5,1)$ , respectively. Figures 11(e) and 11(f) show wave-vector scans at the expected resonance energies for  $Q=(0.5,0.5,0)$  and  $(0.5,0.5,1)$ . In both cases, we find clear intensity enhancement below  $T_c$ . The negative slope in the data may arise from low  $2\theta$  angle in the scattering process. The temperature-dependent scattering at  $Q=(0.5,0.5,0)$  and

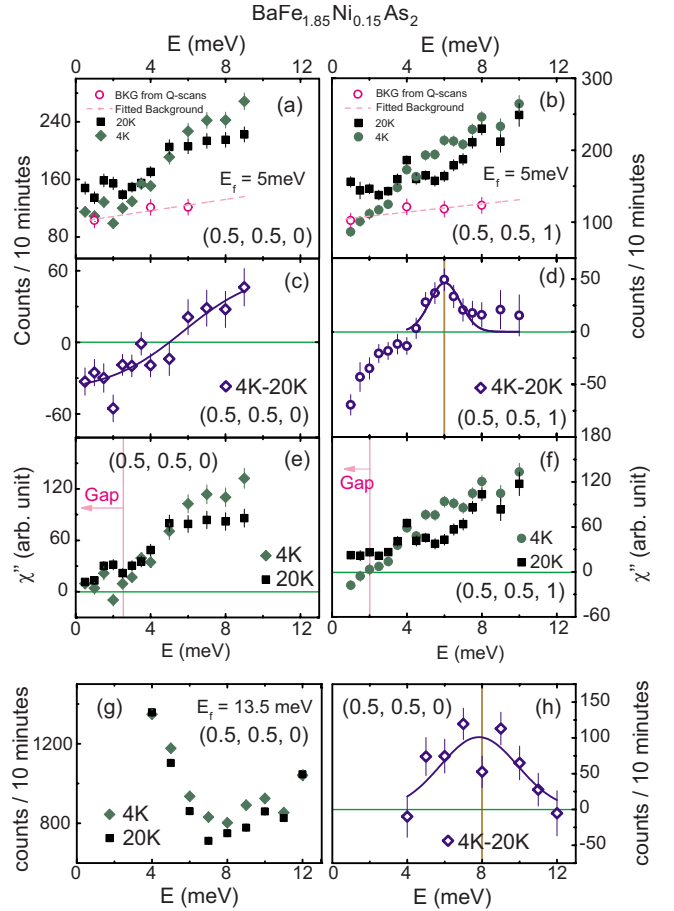


FIG. 10. (Color online) Summary of constant- $Q$  scans at various temperatures for  $\text{BaFe}_{1.85}\text{Ni}_{0.15}\text{As}_2$  with  $E_f=5$  and 13.5 meV. (a) Energy dependence of scattering at  $Q=(0.5,0.5,0)$  above and below  $T_c$ . The scattering shows a clear drop in intensity below  $E=4$  meV and enhancement around 8 meV. One can only probe magnetic scattering below  $E=9$  meV due to kinematic constraints with  $E_f=5$  meV. Circles are background scattering estimated from constant-energy scans at  $E=1, 4,$  and  $6$  meV. (b) Energy dependence of the scattering above and below  $T_c$ , now at  $Q=(0.5,0.5,1)$ . (c) Temperature difference plot between 4 and 20 K showing the intensity gain below  $T_c$  near  $E=8$  meV. (d) Temperature difference data confirm the formation of the neutron spin resonance at  $E=6$  meV. (e) Our estimated  $\chi''(Q,\omega)$  for  $\text{BaFe}_{1.85}\text{Ni}_{0.15}\text{As}_2$  above and below  $T_c$  at  $Q=(0.5,0.5,0)$ , after subtracting the background and correcting for the Bose factor. The magnitude of the superconducting spin gap is about  $E\approx 2.5$  meV. (f)  $\chi''(Q,\omega)$  for  $\text{BaFe}_{1.85}\text{Ni}_{0.15}\text{As}_2$  above and below  $T_c$  at  $Q=(0.5,0.5,1)$ . The system again has a spin gap of  $\sim 2$  meV in the superconducting state. (g) Identical scan as that of (a) except we used  $E_f=13.5$  meV. Superconductivity-induced neutron spin resonance can now be seen around  $E=8$  meV. (h) Temperature difference plot confirms the presence of the resonance at  $E=8$  meV.

$E=8$  meV in Fig. 11(g) shows clear order-parameter-like intensity increase below  $T_c$ , thus confirming the neutron spin resonance.<sup>19-22,24-26</sup>

Finally, we summarize in Fig. 12 the electron-doping dependence of the neutron spin resonance at  $Q=(0.5,0.5,0)$  and  $(0.5,0.5,1)$  as a function of  $T_c$  for both  $\text{BaFe}_{2-x}\text{Ni}_x\text{As}_2$  (Refs. 21, 22, 43, and 46) and  $\text{BaFe}_{2-x}\text{Co}_x\text{As}_2$ .<sup>20,24-26</sup> For

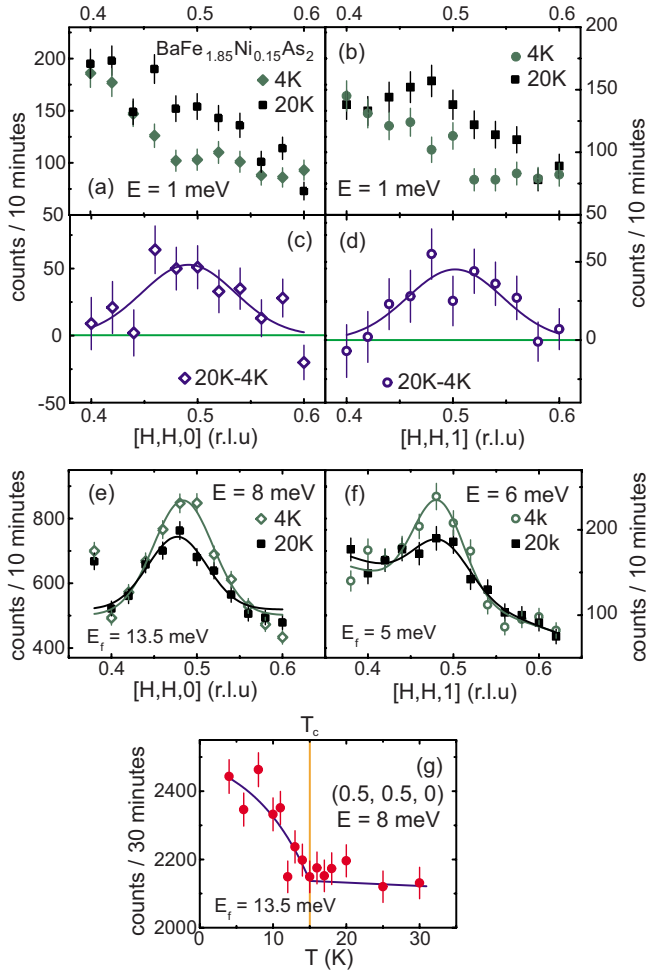


FIG. 11. (Color online) Summary of constant-energy scans at an energy below the spin gap energy and at the resonance energy below and above  $T_c$ . (a)  $Q$  scan along the  $[H,H,0]$  direction below and above  $T_c$  at  $E=1$  meV. There is a clear peak centered at  $(0.5,0.5,0)$  that disappears below  $T_c$ , thus suggesting the opening of a spin gap at  $E=1$  meV and  $(0.5,0.5,0)$ . (b) Similar scan along the  $[H,H,1]$  direction, again indicating the opening a spin gap at  $E=1$  meV and  $(0.5,0.5,1)$ . [(c) and (d)] Temperature-difference plots confirm that superconductivity-induced spin gaps occur at  $(0.5,0.5,0)$  and  $(0.5,0.5,1)$  positions. (e) Constant-energy scans along the  $[H,H,0]$  direction below and above  $T_c$  at the resonance energy of  $E=8$  meV. (f) Similar scans at  $E=6$  meV along the  $[H,H,1]$  direction. In both cases, we find that superconductivity-induced changes happen at the expected wave vectors. (g) Temperature dependence of the scattering at  $E=8$  meV and  $Q=(0.5,0.5,0)$ . Data show clear order-parameter-like increase below  $T_c$ , a hallmark of the neutron spin resonance.

copper oxide high- $T_c$  superconductors, one of the hallmarks of the resonance is that its energy is proportional to  $T_c$  over a very wide temperature range.<sup>32,33</sup> Since  $\text{BaFe}_{2-x}\text{Ni}_x\text{As}_2$  has two resonances at distinctively different energies, its dispersion along the  $c$  axis is related to the superconducting gap  $\Delta_0$  and its deviation  $\delta$  via  $E(Q_z) \sim 2\Delta_0 - 2\delta|\sin(Q_z/2)|$ .<sup>21</sup> The observation of a linear relationship for both mode energies and  $T_c$  suggests that  $\delta/\Delta_0 = [\omega(0.5,0.5,0) - \omega(0.5,0.5,1)]/\omega(0.5,0.5,0)$  is approximately 0.28 and weakly Ni-doping dependent. Therefore, the ratio of inter-

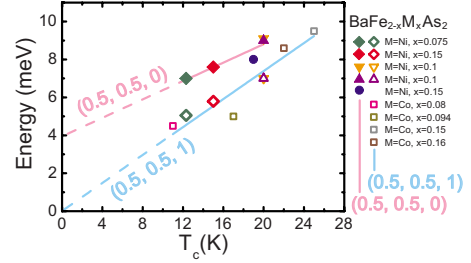


FIG. 12. (Color online) Summary of electron doping dependence of the neutron spin resonance energies at  $Q=(0.5,0.5,0)$  and  $(0.5,0.5,1)$  as a function of  $T_c$ . Data for  $\text{BaFe}_{2-x}\text{Ni}_x\text{As}_2$  are from Refs. 21, 22, 43, and 46 and present work. Data for  $\text{BaFe}_{2-x}\text{Co}_x\text{As}_2$  are from Refs. 20 and 24–26. Solid lines are linear fits to the data.

plane ( $J_\perp$ ) and intraplane ( $J_\parallel$ ) AF couplings,  $J_\perp/J_\parallel$ , is weakly electron-doping dependent assuming that the values of  $\Delta_0$  and  $\delta$  are proportional to  $J_\parallel$  and  $J_\perp$ , respectively.

We now discuss the physical interpretation of the above results. In the theory of spin-fluctuation-mediated superconductivity,<sup>9–13</sup> the electron pairing arises from sign-reversed  $S$ -wave interband scattering between hole pockets centered at the  $\Gamma$  point and electron pockets at the  $M$  points [inset in Fig. 1(a)].<sup>15–18</sup> One of the consequences of such electron-hole pocket excitations is to induce a resonance peak at the AF ordering wave vector  $Q=(0.5,0.5,0)$  in the spin excitations spectrum. In the strictly two-dimensional model, the energy of the resonance is at (or slightly less than) the addition of hole ( $\Delta_0^h$ ) and electron ( $\Delta_0^e$ ) superconducting gap energies ( $\Delta_0 = \Delta_0^h + \Delta_0^e$ ). Our previous finding of three dimensionality of the resonance in optimally doped  $\text{BaFe}_{1.9}\text{Ni}_{0.1}\text{As}_2$  (Refs. 21 and 22) suggests that the superconducting gap energy  $\Delta_0$  should be three dimensional as well and sensitive to the  $Q$  values along the  $c$  axis. The results reported in the present paper on underdoped  $\text{BaFe}_{1.925}\text{Ni}_{0.075}\text{As}_2$  and overdoped  $\text{BaFe}_{1.85}\text{Ni}_{0.15}\text{As}_2$  confirm the earlier conclusion and reveal that the three-dimensional nature of the superconducting gap is prevalent throughout the superconducting dome. If spin excitations are mediating the electron pairing for superconductivity, these results would suggest that the AF exchange coupling along the  $c$  axis ( $J_\perp$ ) contributes significantly to the electron pairing. Although the overall spin excitations as a function of increasing electron doping transform into quasi-two-dimensional spin excitations rather rapidly as demonstrated by the disappearing anisotropic spin gaps at  $Q=(0.5,0.5,0)$  and  $(0.5,0.5,1)$  with increasing Ni doping,<sup>43</sup> the superconductivity-induced resonance retains its three-dimensional character even in the overdoped regime. This means that the superconducting electronic gaps in the iron-arsenic-based materials are three dimensional and quite different from that of the copper oxide superconductors.

#### IV. CONCLUSIONS

In summary, we have determined the doping evolution of the low-energy spin excitations in  $\text{BaFe}_{2-x}\text{Ni}_x\text{As}_2$  for both underdoped and overdoped superconductors. In underdoped  $\text{BaFe}_{1.925}\text{Ni}_{0.075}\text{As}_2$ , we find that the appearance of bulk su-

perconductivity is associated with the appearance of a weak three-dimensional neutron spin resonance. The spectral weight gain of the resonance below  $T_c$  is a rather small portion of the overall normal state magnetic scattering and is compensated by a reduction in the static magnetic moment. Our Ni-doping-dependent investigation of the spin gap and neutron spin resonance reveals that the three-dimensional nature of the mode found earlier for the optimally doped sample is a universal property of Ni-doped superconductors. These results in turn suggest that AF spin excitations between the layers are also important for the superconductivity of these materials.

## ACKNOWLEDGMENTS

We thank Jiangping Hu and Tao Xiang for helpful discussions. The neutron scattering part of this work at UT/ORNL is supported by the U.S. NSF under Grant No. DMR-0756568 and by the U.S. DOE, Division of Scientific User Facilities. The single-crystal growth effort at UT is supported by U.S. DOE BES under Grant No. DE-FG02-05ER46202. The single-crystal growth and neutron-scattering work at IOP is supported by Chinese Academy of Sciences and 973 Program (Grant No. 2010CB833102).

\*slli@aphy.iphys.ac.cn

†daip@ornl.gov

- <sup>1</sup>Y. Kamihara, T. Watanabe, M. Hirano, and H. Hosono, *J. Am. Chem. Soc.* **130**, 3296 (2008).
- <sup>2</sup>M. Rotter, M. Tegel, and D. Johrendt, *Phys. Rev. Lett.* **101**, 107006 (2008).
- <sup>3</sup>L. J. Li, Y. K. Luo, Q. B. Wang, H. Chen, Z. Ren, Q. Tao, Y. K. Li, X. Lin, M. He, Z. W. Zhu, G. H. Cao, and Z. A. Xu, *New J. Phys.* **11**, 025008 (2009).
- <sup>4</sup>S. L. Bud'ko, N. Ni, and P. C. Canfield, *Phys. Rev. B* **79**, 220516(R) (2009).
- <sup>5</sup>C. de la Cruz, Q. Huang, J. W. Lynn, J. Li, W. Ratcliff II, J. L. Zarestky, H. A. Mook, G. F. Chen, J. L. Luo, N. L. Wang, and P. Dai, *Nature (London)* **453**, 899 (2008).
- <sup>6</sup>J. Zhao, Q. Huang, C. de la Cruz, S. Li, J. W. Lynn, Y. Chen, M. A. Green, G. F. Chen, G. Li, Z. Li, J. L. Luo, N. L. Wang, and P. Dai, *Nat. Mater.* **7**, 953 (2008).
- <sup>7</sup>Q. Huang, Y. Qiu, W. Bao, M. A. Green, J. W. Lynn, Y. C. Gasparovic, T. Wu, G. Wu, and X. H. Chen, *Phys. Rev. Lett.* **101**, 257003 (2008).
- <sup>8</sup>J. Zhao, W. Ratcliff II, J. W. Lynn, G. F. Chen, J. L. Luo, N. L. Wang, J. Hu, and P. Dai, *Phys. Rev. B* **78**, 140504(R) (2008).
- <sup>9</sup>I. I. Mazin, D. J. Singh, M. D. Johannes, and M. H. Du, *Phys. Rev. Lett.* **101**, 057003 (2008).
- <sup>10</sup>A. V. Chubukov, *Physica C* **469**, 640 (2009).
- <sup>11</sup>F. Wang, H. Zhai, Y. Ran, A. Vishwanath, and D.-H. Lee, *Phys. Rev. Lett.* **102**, 047005 (2009).
- <sup>12</sup>V. Cvetkovic and Z. Tesanovic, *EPL* **85**, 37002 (2009).
- <sup>13</sup>A. Moreo, M. Daghofer, J. A. Riera, and E. Dagotto, *Phys. Rev. B* **79**, 134502 (2009).
- <sup>14</sup>I. I. Mazin and J. Schmalian, *Physica C* **469**, 614 (2009).
- <sup>15</sup>T. A. Maier and D. J. Scalapino, *Phys. Rev. B* **78**, 020514(R) (2008).
- <sup>16</sup>T. A. Maier, S. Graser, D. J. Scalapino, and P. Hirschfeld, *Phys. Rev. B* **79**, 134520 (2009).
- <sup>17</sup>M. M. Korshunov and I. Eremin, *Phys. Rev. B* **78**, 140509(R) (2008).
- <sup>18</sup>K. Seo, C. Fang, B. A. Bernevig, and J. Hu, *Phys. Rev. B* **79**, 235207 (2009).
- <sup>19</sup>A. D. Christianson, E. A. Goremychkin, R. Osborn, S. Rosenkranz, M. D. Lumsden, C. D. Malliakas, I. S. Todorov, H. Claus, D. Y. Chung, M. G. Kanatzidis, R. I. Bewley, and T. Guidi, *Nature (London)* **456**, 930 (2008).
- <sup>20</sup>M. D. Lumsden, A. D. Christianson, D. Parshall, M. B. Stone, S. E. Nagler, G. J. MacDougall, H. A. Mook, K. Lokshin, T. Egami, D. L. Abernathy, E. A. Goremychkin, R. Osborn, M. A. McGuire, A. S. Sefat, R. Jin, B. C. Sales, and D. Mandrus, *Phys. Rev. Lett.* **102**, 107005 (2009).
- <sup>21</sup>S. Chi, A. Schneidewind, J. Zhao, L. W. Harriger, L. Li, Y. Luo, G. Cao, Zhuang Xu, M. Loewenhaupt, J. Hu, and P. Dai, *Phys. Rev. Lett.* **102**, 107006 (2009).
- <sup>22</sup>S. Li, Y. Chen, S. Chang, J. W. Lynn, L. Li, Y. Luo, G. Cao, Z. Xu, and P. Dai, *Phys. Rev. B* **79**, 174527 (2009).
- <sup>23</sup>D. Parshall, K. A. Lokshin, J. Niedziela, A. D. Christianson, M. D. Lumsden, H. A. Mook, S. E. Nagler, M. A. McGuire, M. B. Stone, D. L. Abernathy, A. S. Sefat, B. C. Sales, D. G. Mandrus, and T. Egami, *Phys. Rev. B* **80**, 012502 (2009).
- <sup>24</sup>D. K. Pratt, W. Tian, A. Kreyssig, J. L. Zarestky, S. Nandi, N. Ni, S. L. Bud'ko, P. C. Canfield, A. I. Goldman, and R. J. McQueeney, *Phys. Rev. Lett.* **103**, 087001 (2009).
- <sup>25</sup>A. D. Christianson, M. D. Lumsden, S. E. Nagler, G. J. MacDougall, M. A. McGuire, A. S. Sefat, R. Jin, B. C. Sales, and D. Mandrus, *Phys. Rev. Lett.* **103**, 087002 (2009).
- <sup>26</sup>D. S. Inosov, J. T. Park, P. Bourges, D. L. Sun, Y. Sidis, A. Schneidewind, K. Hradil, D. Haug, C. T. Lin, B. Keimer, and V. Hinkov, *Nat. Phys.* **6**, 178 (2010).
- <sup>27</sup>O. Lipscombe, L. Harriger, P. Freeman, M. Enderle, C. Zhang, M. Wang, T. Egami, J. Hu, T. Xiang, M. Norman, and P. Dai, [arXiv:1003.1926](https://arxiv.org/abs/1003.1926) (unpublished).
- <sup>28</sup>J. Rossat-Mignod, L. P. Regnault, C. Vettier, P. Bourges, P. Bulet, J. Bossy, J. Y. Henry, and G. Lapertot, *Physica C* **185-189**, 86 (1991).
- <sup>29</sup>P. Dai, H. A. Mook, R. D. Hunt, and F. Doğan, *Phys. Rev. B* **63**, 054525 (2001).
- <sup>30</sup>H. F. Fong, B. Keimer, D. Reznik, D. L. Milius, and I. A. Aksay, *Phys. Rev. B* **54**, 6708 (1996).
- <sup>31</sup>C. Stock, W. J. L. Buyers, R. Liang, D. Peets, Z. Tun, D. Bonn, W. N. Hardy, and R. J. Birgeneau, *Phys. Rev. B* **69**, 014502 (2004).
- <sup>32</sup>S. D. Wilson, P. Dai, S. Li, S. Chi, H. J. Kang, and J. W. Lynn, *Nature (London)* **442**, 59 (2006).
- <sup>33</sup>J. Zhao, P. Dai, S. Li, P. G. Freeman, Y. Onose, and Y. Tokura, *Phys. Rev. Lett.* **99**, 017001 (2007).
- <sup>34</sup>J. Zhao, D.-X. Yao, S. Li, T. Hong, Y. Chen, S. Chang, W. Ratcliff II, J. W. Lynn, H. A. Mook, G. F. Chen, J. L. Luo, N. L. Wang, E. W. Carlson, J. Hu, and P. Dai, *Phys. Rev. Lett.* **101**,

- 167203 (2008).
- <sup>35</sup>R. A. Ewings, T. G. Perring, R. I. Bewley, T. Guidi, M. J. Pitcher, D. R. Parker, S. J. Clarke, and A. T. Boothroyd, *Phys. Rev. B* **78**, 220501(R) (2008).
- <sup>36</sup>R. J. McQueeney, S. O. Diallo, V. P. Antropov, G. D. Samolyuk, C. Broholm, N. Ni, S. Nandi, M. Yethiraj, J. L. Zarestky, J. J. Pulikkotil, A. Kreyssig, M. D. Lumsden, B. N. Harmon, P. C. Canfield, and A. I. Goldman, *Phys. Rev. Lett.* **101**, 227205 (2008).
- <sup>37</sup>K. Matan, R. Morinaga, K. Iida, and T. J. Sato, *Phys. Rev. B* **79**, 054526 (2009).
- <sup>38</sup>S. O. Diallo, V. P. Antropov, T. G. Perring, C. Broholm, J. J. Pulikkotil, N. Ni, S. L. Bud'ko, P. C. Canfield, A. Kreyssig, A. I. Goldman, and R. J. McQueeney, *Phys. Rev. Lett.* **102**, 187206 (2009).
- <sup>39</sup>J. Zhao, D. T. Adroja, D.-X. Yao, R. Bewley, S. Li, X. F. Wang, G. Wu, X. H. Chen, J. Hu, and P. Dai, *Nat. Phys.* **5**, 555 (2009).
- <sup>40</sup>J.-H. Chu, J. G. Analytis, C. Kucharczyk, and I. R. Fisher, *Phys. Rev. B* **79**, 014506 (2009).
- <sup>41</sup>C. Lester, J.-H. Chu, J. G. Analytis, S. C. Capelli, A. S. Erickson, C. L. Condon, M. F. Toney, I. R. Fisher, and S. M. Hayden, *Phys. Rev. B* **79**, 144523 (2009).
- <sup>42</sup>P. C. Canfield, S. L. Bud'ko, Ni Ni, J. Q. Yan, and A. Kracher, *Phys. Rev. B* **80**, 060501(R) (2009).
- <sup>43</sup>L. W. Harriger, A. Schneidewind, S. Li, J. Zhao, Z. Li, W. Lu, X. Dong, F. Zhou, Z. Zhao, J. Hu, and P. Dai, *Phys. Rev. Lett.* **103**, 087005 (2009).
- <sup>44</sup>S. Diallo, D. Pratt, R. Fernandes, W. Tian, J. Zarestky, M. Lumsden, T. Perring, C. Broholm, N. Ni, S. Bud'ko, P. Canfield, H. Li, D. Vaknin, A. Kreyssig, A. Goldman, and R. McQueeney, [arXiv:1001.2804](https://arxiv.org/abs/1001.2804) (unpublished).
- <sup>45</sup>W. Ratcliff II, P. A. Kienzle, J. W. Lynn, S. Li, P. Dai, G. F. Chen, and N. L. Wang, *Phys. Rev. B* **81**, 140502(R) (2010).
- <sup>46</sup>J. Zhao, L. P. Regnault, C. Zhang, M. Wang, Z. Li, F. Zhou, Z. Zhao, Chen Fang, Jiangping Hu, and P. Dai, *Phys. Rev. B* **81**, 180505(R) (2010).